International Journal of Biological Macromolecules 213 (2022) 944–954

Contents lists available at ScienceDirect

International Journal of Biological Macromolecules

journal homepage: www.elsevier.com/locate/ijbiomac

Naringenin as a potential inhibitor of human cyclin-dependent kinase 6: Molecular and structural insights into anti-cancer therapeutics

Mohd Yousuf [a], Anas Shamsi [b], Shama Khan [c], Parvez Khan [b], Moyad Shahwan [d], Abdelbaset Mohamed Elasbali [e,f,*], Qazi Mohd Rizwanul Haque [a], Md. Imtaiyaz Hassan [b,*]

[a] Department of Biosciences, Jamia Millia Islamia, Jamia Nagar, New Delhi, India
[b] Centre for Interdisciplinary Research in Basic Sciences, Jamia Millia Islamia, Jamia Nagar, New Delhi 110025, India
[c] Vaccines and Infectious Disease Analytics (VIDA), University of the Witwatersrand, Johannesburg, South Africa
[d] Centre of Medical and Bio-Allied Health Sciences Research, Ajman University, United Arab Emirates
[e] Department of Clinical Laboratory Science, College of Applied Sciences-Qurayyat, Jouf University, Sakaka, Saudi Arabia
[f] Department of Pathology, Faculty of Medicine, University of Benghazi, Benghazi-Libya

ARTICLE INFO

Keywords:
Kinase inhibitors
cancer therapeutics
Fluorescence binding
Molecular dynamics simulation
Isothermal titration calorimetry

ABSTRACT

Cancer is one of the major causes of global deaths and needs immediate therapeutic development. So far, several strategies have been undertaken to prevent cancer, including kinase targeting by small-molecule inhibitors. Cyclin dependent kinase 6 (CDK6) plays an essential role in cancer progression and development as its over-expression is associated with tumor development and progression. The present study demonstrated that Naringenin (NAG) binds strongly to CDK6 with a binding affinity of −7.51 kcal/mol. ATPase assay of CDK6 in the presence of NAG shows that it inhibits CDK6 with an IC_{50} = 3.13 μM. Fluorescence and isothermal titration calorimetry studies demonstrated that NAG binds to CDK6 with the binding constant (*K*) values of 3.55×10^6 M^{-1} and $7.06 \pm 2.70 \times 10^6$ M^{-1}, respectively. The cell-based functional studies showed that NAG decreases the cell viability of human cancer cell lines, induces apoptosis, and reduces their colonization ability. Outcomes of the present *in silico* and *in vitro* studies highlighted the significance of NAG for the development of anti-cancer leads in terms of CDK6 inhibitors and provided future implications for combinatorial anti-cancer therapies.

1. Introduction

Human cells share the standard features of cell growth and survival, but the mechanisms of action and their development process are different. Proper coordination is found in cell proliferation and development [1,2]. Several proteins are involved in various cellular signaling pathways that maintain cell growth, survival, and development [3]. Post-translational modification is one of the most important processes required for the structural and functional activities of the proteins [4]. Accumulation of mutations is usual process during the cell division. But sometimes mutations changes a protein's structure and function, causing the alterations in several cellular pathways and are responsible for developing disease conditions [5–8].

Phosphorylation is a post-translation modification process carried out by protein kinases [9]. More than 80 % of cellular pathways are regulated by protein kinase. CDKs belong to the Ser/Thr family of protein kinases that maintain cell growth and development [10]. Several checkpoints are available for the orderly transition from one stage to another cell cycle stage [11,12]. CDK6 interacts with other partner molecules during the first cell cycle stage and controls cell proliferation. CDK6 interacts with Cyclin-D and activates it reversibly during cell growth and development. CDK6 inactivates the retinoblastoma (RB), a tumor suppression protein, through phosphorylation and regulates cell cycle progression [13,14]. Hyper phosphorylation of RB protein leads to the dissociation of the Rb-E_2F complex. The freeform of E_2F (Eukaryotic Transcription Factor) directly regulates all signaling pathway responsible for the cell cycle transition from G1 to S phase. In most cancers, the aberrant activation of CDK6 is observed [14,15]. Upregulation of CDK6 is responsible for the permanent activation of the Rb-E2F pathway in an irreversible manner that results in continuous growth and development

Abbreviations: CDK6, Cyclin dependent kinase 6; ITC, Isothermal titration calorimetry; NAG, Naringenin; MM/GBSA, Molecular Mechanics/Generalized-Born Surface Area; DCCM, Dynamic cross-correlation matrix.

* Corresponding authors.
E-mail addresses: aeelasbali@ju.edu.sa (A.M. Elasbali), mihassan@jmi.ac.in (Md.I. Hassan).

https://doi.org/10.1016/j.ijbiomac.2022.06.013
Received 29 April 2022; Received in revised form 28 May 2022; Accepted 5 June 2022
Available online 8 June 2022

of cancer cells [16]. Besides this, upregulation of CDK6 helps in metabolic switching by inhibiting glycolysis and activating other metabolic pathways. One of them is the pentose phosphate pathway (PPP), the serine pathway that prevents the cancer cell from skipping the apoptotic pathways [17,18]. These studies suggest that CDK6 targeting using small molecular inhibitors is a potential therapeutic approach to develop cancer therapies.

According to the known hallmarks of cancer, the FDA has approved several drugs to treat cancer [19]. To inhibit the cell proliferation in cancer cells, abemaciclib, palbociclib or ribociclib are used for the CDK6 targeted anti-cancer therapies. These drugs interact with CDK6 and prevent the cell transition from G1 to the S phase cell cycle [20,21]. Due to continuous mutations and CDK6 over expression cancer cells develop drug resistance and possess RB in inactive state (phospho-RB or RB null) [22,23]. Abemaciclib, palbociclib, or ribociclib drugs are only effective against the RB^{+} cancer cells. So more exploration is required for the development of CDK6-directed cancer therapies.

Natural products are used in traditional /folk medicine-based cancer therapies for several decades [24–28]. Secondary metabolites of plants are the source of polyphenolic compounds, including flavonoids. Several studies reported that flavonoids have anti-cancer activity. They act as anti-carcinogen and prevent the proliferation of cancer cells [29–32]. Several flavonoids are isolated from the plants and checked for their anti-cancer effect on cancer cells to identify the mechanism of action. Recent studies suggest that flavonoids act as anti-oxidant molecules that regulate ROS production, leading to cell apoptosis in cancer cells, and preventing DNA damage from the cellular oxidation process in normal cells [33,34].

Naringenin (NAG) is a flavonoid, widely distributed in several fruits and vegetables such as citrus, tomato, and bergamot [35–38]. *In vitro and in vivo* studies suggest that NAG shows anti-oxidant and anti-inflammatory activity and can be used to treat hepatitis, lung injury, diabetes, atherosclerosis, obesity and cancer with minimum systematic cell toxicity [39–47]. Preclinical studies showed that NAG could be used to treat most cancers, including prostate, breast, pancreatic, gastric, and lung cancer [48,49]. NAG targeting the signaling pathways of the AKT, ERK, RTK receptor, NF-κB, TGF-β1, and MAPK, induce apoptosis and prevent cancer cell proliferation [47,50–52]. In some cancer types such as breast cancer, NAG reverts multi-drug resistance properties of cancer cells [53–55]. Although NAG efficacy against tumor growth and metastasis is well-established, the mechanism of action is still unexplored.

Furthermore, cellular and molecular level studies are required to reveal the intracellular target molecules of NAG for cancer treatment. It would provide newer insights into the anti-cancer activity of NAG. Studying the binding of NAG to the CDK6 offers a better understanding of the mechanism of action.

NAG interacts with CDK6 and subsequently inhibits the proliferation of cancer cells. Previously, we have reported the antitumor activity of NAG as a pyruvate dehydrogenase kinase (PDK) inhibitor [56]. However, the present study focused on the anti-cancer activity of NAG against CDK6, establishing that NAG also targets CDK6 and can be used to develop multi-targeted anti-cancer therapies. *In-silico and in-vitro* experiments were performed to investigate the interaction pattern, binding constant, and stability of the CDK6 with NAG.

2. Materials and methods

2.1. Chemical and reagents

Pure Yield™ Plasmid Midi prep System (Cat no. A2495) and PCR Clean-Up System (Cat no A9281) for the Plasmid isolation and gel extraction, respectively, were procured from Promega Corporation Madison, USA. Fast digestion Restriction endonuclease *Nco*I, *Xho*I, and ligation enzyme were purchased from Thermo Fisher Scientific (USA). DifcoTM LB broth Miller for bacterial growth culture was obtained from BD Biosciences (USA). Kanamycin sulfate was obtained from Duchefa Biochiem (Netherlands). IPTG (Isopropyl β-D-1-thiogalactopyranoside), PMSF (Phenylmethylsulfonyl fluoride) and NAG were purchased from MP biomedical (USA).

2.2. Cloning expression and purification

pC-DNA containing CDK6 gene was procured from Harvard Medical repository unit (USA) and amplified by specific primers through PCR (Thermal cycler-Bio Red). PCR amplified product of CDK6 gene has *NcoI* and *XhoI* restriction digestion sites on both ends. Digested CDK6 gene was ligated into the pET28a + prokaryotic cloning vector. Restriction digestion and DNA sequencing methods were used to verify the final clone. CDK6 clone was transformed into *E. coli BL21* ($codon^{+}$) bacterial cells and kanamycin were used as selection markers. Overnight bacterial culture (Primary culture) was grown at 37 °C till the OD_{600} reached 0.6. IPTG-induced bacterial culture was incubated for 16 h at 18 °C. The next day culture was subjected to centrifugation (10,000 rpm) for 10 min. We purified the CDK6 protein from Inclusion bodies (IBs) by Ni-NTA column chromatography as per our standard protocol [57]. A kinase activity assay was performed to check the activity of purified protein.

2.3. Fluorescence based binding assay

To study NAG binding affinity and pattern with CDK6 protein, a fluorescence binding experiment was performed using Jasco spectrofluorimeter (FP-6200) containing thermostat Peltier device to maintain the temperature at 25 ± 0.1 °C. A fluorescence experiment was carried out in a 5 mm quartz cuvette. CDK6 was excited at 280 nm, and emission spectra were recorded between 300 and 400 nm [1]. The emission and excitation slit widths were fixed at 10 nm at the medium response. The stock solution of NAG was prepared, and purified CDK6 protein was titrated (0–9 nM). Fluorescence quenching data was evaluated using earlier published protocols' modified Stern Volmer equation [2] (Eq. (1)) as described below:

$$log\frac{F_0 - F}{F} = logK + nlog[C] \quad (1)$$

F_0 and F refer to fluorescence intensity in the absence and presence of ligands. The binding constant and the number of binding sites are represented by K and n. The concentration of ligand is represented by C.

2.4. Kinase inhibition assay

ATPase assay was performed to determine the kinase activity of CDK6, which depends on the free form of inorganic phosphate (P_i) released during the hydrolysis of ATP. To optimize the CDK6 protein and ATP concentrations, we first used the fixed amount of ATP and varied the CDK6 protein concentrations (1–10 μM). After optimizing the protein concentration, kinase activity was measured at different concentrations of ATP (50–200 μM) with constant protein (5 μM) concentration. Positive control of protein was also used to measure the concentration of Pi released by the hydrolysis of ATP [58,59]. To determine the effect of drug molecules on the CDK6 kinase activity, we perform the experiments in the presence of gradually increasing NAG concentrations [57,60,61].

2.5. Isothermal titration calorimetry

The isothermal titration calorimetry (GE, MicroCal, USA) experiment was performed to measure the binding affinity of NAG with the CDK6. Briefly, the purified CDK6 protein and the NAG were dissolved in the dialyzed buffer (25 mM Tris pH 8.0, 200 mM $MgCl_2$) and adequately degassed. The sample cell contained a 20 μM concentration of CDK6 protein (2 ml), while a 200 μM concentration of NAG (0.5 ml) was present in the syringe. There was a programmed titration, in which the

first injection of 5 μl was a false one, followed by successive injections of 10 μl ligand into the sample cell with spacing set at 180 s. The MicroCal Origin 8.0 was used to analyze the stoichiometry of binding (n), enthalpy change (ΔH), and an association constant (K_a) [62,63].

2.6. Protein-ligand docking system set-up

The 2.1 Å crystal structure of CDK6 protein (PDB code: 3NUP https://www.rcsb.org/structure/3NUP), was downloaded from the Protein Data Bank. Schrödinger package [64] was used to perform all preliminary removal of crystallographic water, hydrogens atoms addition, setting of charge to neutral pH (7.0), and identifying appropriate ionization states for all amino acid residues in the CDK6 structure.

The structure of NAG with PubChem CID number 932 was retrieved. Schrödinger's LigPrep module was chosen to prepare the NAG structure following the additions of accurate hydrogen atoms and optimizing the orientation. The extra precision mode of the Glide module [62] in Schrödinger accounted for molecular docking findings. Receptor grid was created with coordinates of X = 22.86 Y = 36.11 Z = −8.56; having proportions of 10 × 10 × 10 Å. As molecular docking is a preliminary assessment to explore the mode of binding of any compound. Further molecular dynamics simulation studies were performed to observe the structural changes in CDK6 protein.

2.7. Molecular dynamics simulations

For MD simulation studies, GPU accelerated simulation engine PMEMD encrypted in the Amber-18 package [65] was accessed from Super Computing Facility. The most recent force-field employed for Amber's package *i.e.*, FF14SB [66] was utilized to parametrize the structure of CDK6 in complex with NAG. TIP3P [66] water box and LEaP module [67] employed in Amber 18 was utilized for ion solvations. Equilibration was performed for 500 ps having 300 K heating temperature. Finally a 200 ns of MD simulations was achieved for the complex and apo CDK6 protein to analyze the structural changes in the protein. The detailed methodolgy have been published in our recent publication [58,59].

2.8. Post-MD simulation dynamic trajectories analysis

The CDK6 and NAG-CDK6 complex trajectories were evaluated using the CPPTRAJ component [68] of Amber 18 package. The structural changes in CDK6 protein were observed in calculating RMSD, RMSF, R_g, SASA, formation of hydrogen bonds, and matrix of amino acid residues. Generating the 2-dimensional graphs from the MD trajectories were achieved by the Origin plotting tool [69].

2.9. Thermodynamic free energy calculations

To calculate the total and comparative binding free energies of the NAG-CDK6 complex, the Molecular Mechanics/Generalized-Born Surface Area (MM/GBSA) method was incorporated [70]. All counter ions and solvents were stripped using the CPPTRAJ module of Amber 18. The binding free energies were measured for the NAG-CDK6 complex as below:

$$\Delta G_{bind} = G_{\text{complex}} - G_{\text{protein}} - G_{\text{ligand}} \quad (2)$$

ΔG_{bind} (free energy) is calculated from the below equations:

$$\Delta G_{bind} = \Delta E_{\text{gas}} + \Delta G_{\text{solvation}} - T\Delta S \quad (3)$$

Where,

$$\Delta E_{\text{gas}} = \Delta E_{\text{int}} + \Delta E_{\text{vdw}} + \Delta E_{\text{elec}} \quad (4)$$

$$\Delta E_{\text{int}} = \Delta \text{E}_{\text{bond}} + \Delta E_{\text{angle}} + \Delta E_{\text{torsion}} \quad (5)$$

$$\Delta G_{solvation,} = \Delta G_{\text{polar}} + G_{\text{nonploar}}, \quad (6)$$

$$\Delta G_{\text{nonploar}} = \gamma \Delta SASA + \beta \quad (7)$$

The $T\Delta S$ is the modification in entropy of ligand binding, which was neglected at this point as it has been observed that the results of entropic influence are frequently not essential when taking binding affinities of ligand (Eq. (3)). The gas-phase energy (ΔE_{gas}) is the sum of internal (ΔE_{int}), van der Waals (ΔE_{vdW}), and Coulombic (ΔE_{elec}) energies (Eq. (4)). The internal energy (ΔE_{int}) is the energy connected with the vibration of bonds, angles and rotation of single bond torsional angles (Eq. (5)). The free solvation energy ($\Delta G_{solvation}$) is the aggregate of polar (ΔG_{polar}) (G_{nonploar}) and non-polar (G_{nonploar}) contributions (Eq. (6)). The contribution of polar solvation (ΔG_{polar}) was measured using the Generalized Born (GB) solvation. However, the non-polar free energy ($\Delta G_{\text{nonploar}}$) contribution was assessed with Eq. (7).

2.10. Cell viability studies

A standard MTT assay was performed to see the effect of NAG treatment on the cell viability of A549 and MCF-7 as described [57,61]. The MCF-7 and A549 cells are routinely cultured in DMEM media supplemented with 10 % FBS and 1 % antibiotic cocktail solution. The cells were not grown for >20–30 passages and routinely checked for mycoplasma contamination to maintain cultural homogeneity. To perform cell viability studies, cells were seeded at a density of 3000–4000 cells/wells in a 96-well cell culture plate and following overnight growth; the cells were treated with NAG (0–1000 μM) for 72 h. Following the incubation time (after 72 h), 10 μl of MTT (from 5 mg/ml stock solution in PBS, pH 7.4) was added to each well of the plate and further incubated at 37 °C for 3–4 h. The mixture of culture media and MTT were aspirated carefully, and the resulting purple formazan was dissolved by adding 100 μl of DMSO. The absorption of the final product was recorded at 570 nm and used to estimate percentage cell viability.

2.11. Colony formation studies

To access the effect of NAG on the clonogenicity of A549 and MCF-7, the cells were seeded (nearly 1000–1200 cells/well) in a 6-well cell culture plate. The cells were allowed to grow for 24–48 h, and each cell type was incubated with 50 μM and 100 μM NAG for 10–12 days (at 37 °C, in a 5 % CO_2 incubator). The control cells were treated with media only or vehicle control. On completing the experiment, the final colonies in each treatment group were fixed through 100 % methanol and stained with crystal violet. ImageJ software quantified the colony count (https://imagej.nih.gov/ij/) and plotted it for comparative analysis.

2.12. Annexin-V/PI staining

Annexin-V/PI staining was used to see the apoptotic potential of NAG as described [61,71]. Cells were seeded in 60 mm cell culture dishes, and once they reached 50–60 confluency, they were treated with the NAG or vehicle control for 48-72 h. The cells were trypsinized, washed twice with PBS, and collected for staining following the NAG treatment. The collected cells were stained with annexin-V-Cy5/PI (BD-Biosciences, San Jose, USA) and analyzed using flow cytometry.

3. Result and discussion

3.1. Molecular docking

To analyze the interactions of NAG with CDK6 using molecular docking, we optimized the three-dimensional structure of NAG using various parameters. An improved orientation of NAG was attained in the active site of CDK6 with enhanced energies of the NAG-CDK6 complex. NAG reported considerable binding energy and thus suggested as a

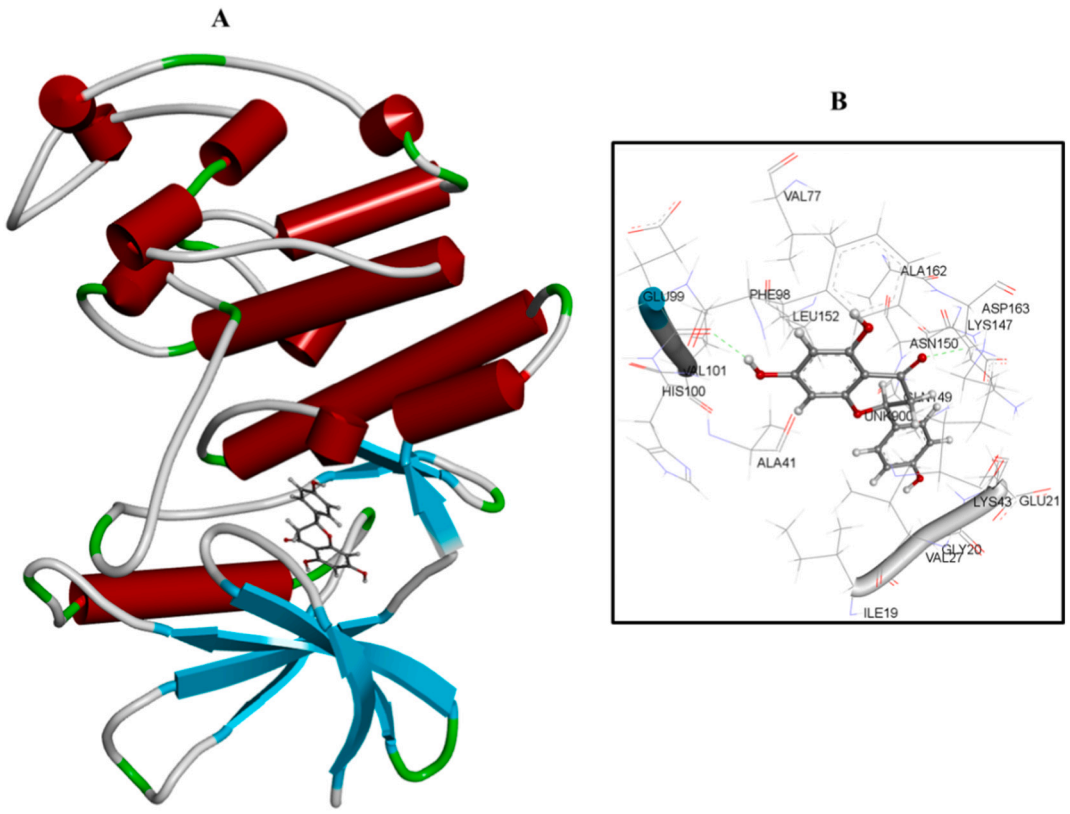

Fig. 1. (A) Structural representation of CDK6 enzyme (schematic view) in complex with NAG (color by atom name). (B) Close-up view of the binding site and binding site residues of CDK6 with NAG.

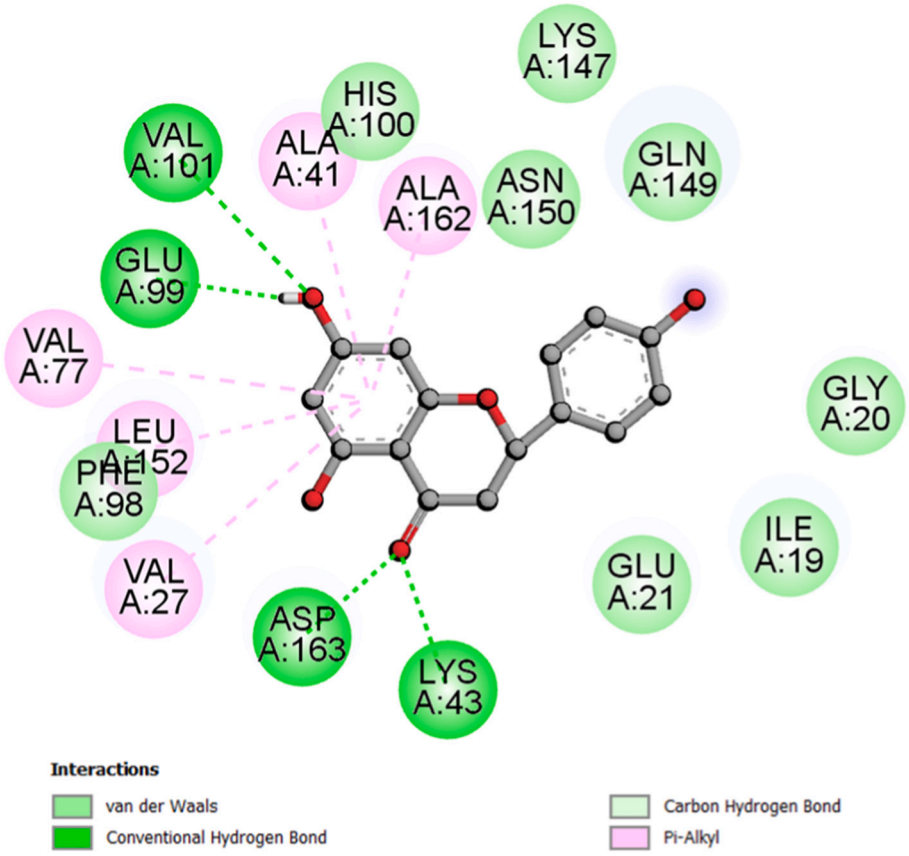

Fig. 2. Docked pose of NAG and molecular interactions of NAG with the binding site of CDK6 enzyme.

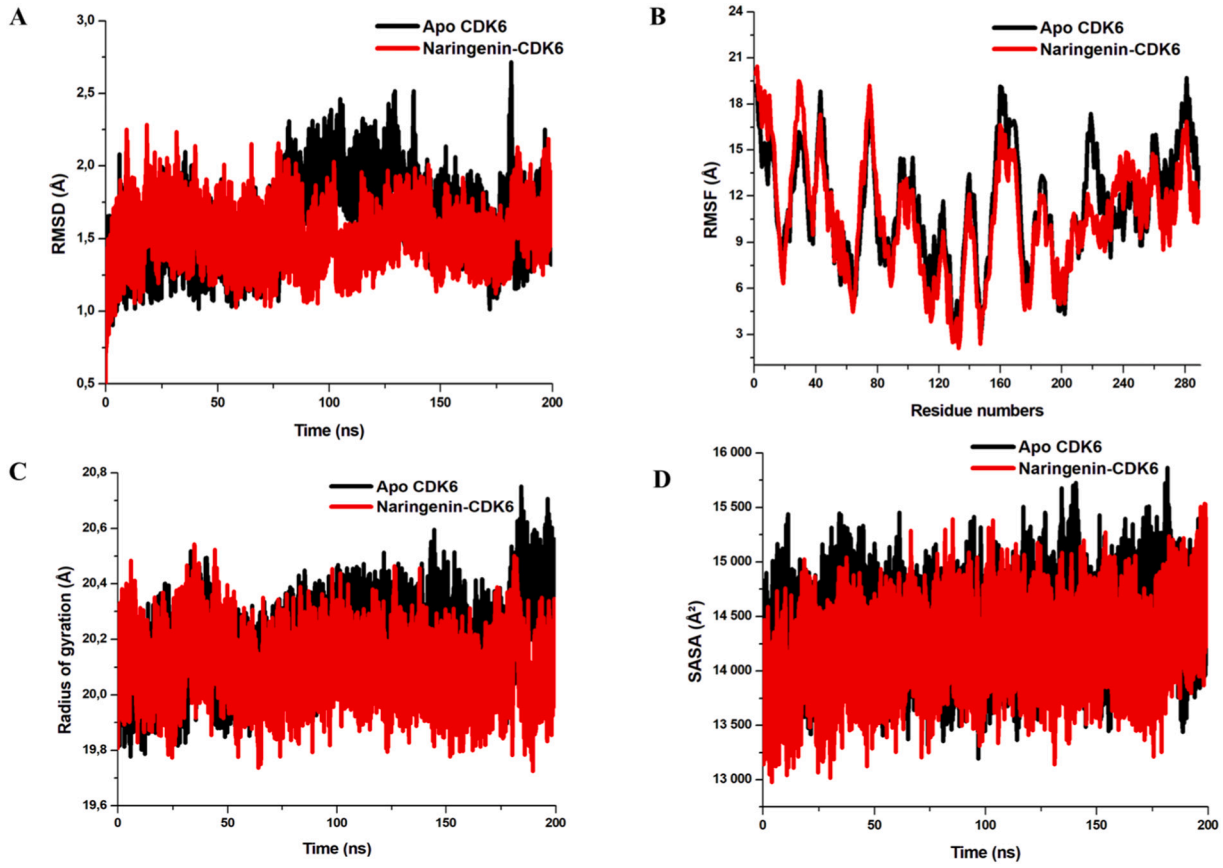

Fig. 3. Structural dynamics of CDK6 apo (black color) and NAG bound CDK6 (red color) enzyme. (A) RMSD, (B) RMSF, (C) R_g values, and (D) SASA values across C^{α} backbone in Å of apo CDK6 and NAG –CDK6 complex in Å across Cα backbone of all the two conditions calculated after 200 ns of MD trajectories. (For interpretation of the references to color in this figure legend, the reader is referred to the web version of this article.)

potential inhibitor of CDK6. Fig. 1 illustrates the output from docking findings of NAG with CDK6. The NAG-CDK6 complex showed a considerable docking score of −7.51 kcal/mol. As shown in Fig. 2, one benzene ring of NAG is involve in binding to CDK6. This ring formed various Pi-alkyl and hydrogen bonds. One hydroxyl group of this ring produced two hydrogen bonds with Glu99 and Val101 residues of CDK6. It has also created a network of five Pi-alkyl interactions with Val27, Ala41, Val77, Leu152 and Ala162. Two more hydrogen bonds were formed with other hydroxyl groups of NAG to Lys43 and Asl163 amino acid residues. These interactions are significantly trustworthy in binding NAG with CDK6 protein with a favorable binding score. Based on these preliminary findings, we decided further to explore the binding mechanism of NAG with CDK6.

3.2. Post-dynamics trajectories analysis

MD simulations were perfromed to investigate the output of docking results [69]. Structural changes were observed in the trajectories attained after 200 ns of MD simulations in all the structural analyses [72–75]. The deviations in RMSD values exposed conformational changes in CDK6 protein after NAG binding. Fig. 3A signifies that after 40 ns, the NAG-CDK6 complex was stabilized and reached convergence. However, the apo CDK6 was stabilized after 40 ns, but fluctuations can be noted again from 80 to 130 ns. NAG-CDK6 complex exposed the minimum RMSD value of 1.89 Å, while CDK6 showed a 2.09 Å score individually. Huge motions in the fluctuations of CDK6 protein were seen, particularly from 80 to 130 ns, before the system reached convergence. As seen from the figure, a stable and steady NAG-CDK6 complex was observed during the whole 200 ns MD trajectories. This finding favors the NAG-CDK6 complex binding by showing the least changes in C^{α} backbone atoms. Further calculations on these trajectories were believed consistent after this structural analysis.

We calculated RMSF for both the systems after the RMSD analysis. The notable fluctuations in amino acid residues of CDK6 and NAG-CDK6 complex are shown in Fig. 3B. Higher C^{α} RMSF scores between 140 and 170 residues were seen in the CDK6 protein; however, similar residues were not fluctuating much in the NAG-CDK6 complex. The total score of RMSF in CDK6 was 12.79 Å, but in NAG-CDK6, it was 11.15 Å. The highly fluctuated residues from 85 to 93 in NAG-CDK6 were observed. These contribute to the binding of NAG to CDK6 protein by exhibiting high mobility in MD simulations, signifying enhanced binding of NAG.

R_g was determined for the residues to examine the solidity of CDK6 protein prior and when NAG binds to CDK6 protein, as displayed in Fig. 3C. The 2D plot indicates that both CDK6 and NAG-CDK6 complex showed compact performance. A slight difference can be noted between these two systems. CDK6 offers an *Rg* value of 20.19 Å, and NAG-CDK6 showed 20.11 Å. This finding proposed better compactness and improved function of NAG after binding to CDK6 protein.

Time-dependent SASA was assessed for the CDK6 and NAG-CDK6 complex from the MD simulations [76]. A precise evaluation of SASA is essential in observing changes associated with natural compounds like NAG [77]. Overall values of SASA for CDK6 and NAG-CDK6 complex were measured from the resultant trajectories, and the 2D plot for this analysis is shown in Fig. 3D. The 14,251 $Å^2$ SASA score was noted in the NAG-CDK6 complex after the complex was exposed to the solvent. A slight increase in the SASA value of CDK6 protein with 14,289 $Å^2$ was reported related to the NAG-CDK6 complex. The NAG-CDK6 showed a better value of SASA. The overall SASA values from the resulting trajectories indicate the folding and unfolding orientations of the NAG-CDK6 complex and suggest enhanced exposure of NAG to solvent with

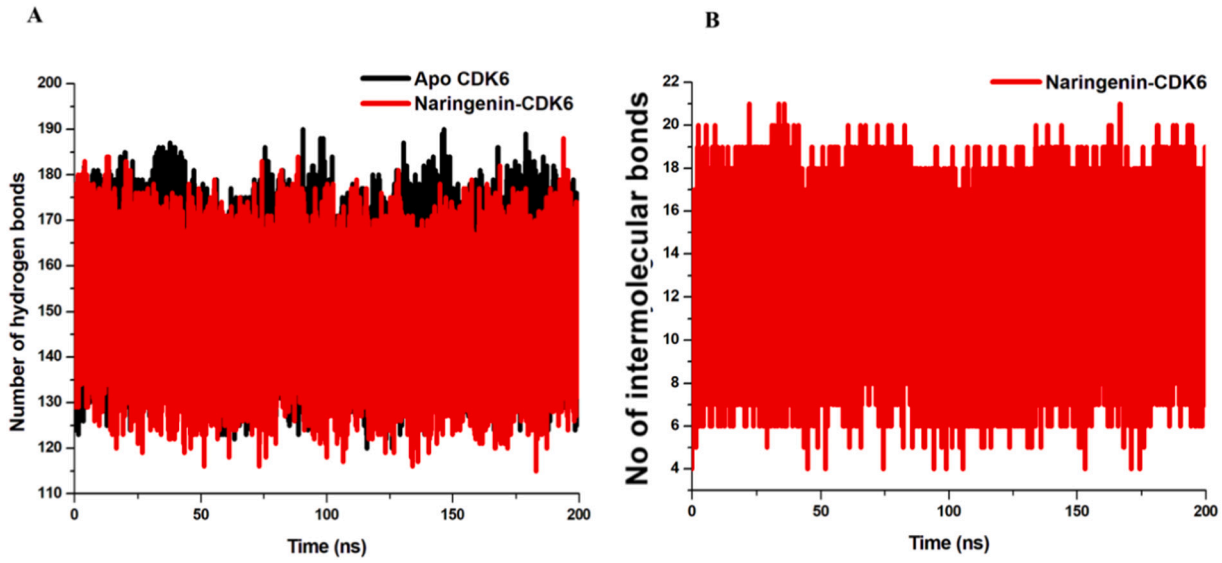

Fig. 4. Hydrogen bond analysis. (A) Intramolecular hydrogen bonds in apo (black color) and NAG-CDK6 complex (red color). (B) Intermolecular hydrogen bonds in NAG bound CDK6 complex calculated after 200 ns MD simulation. (For interpretation of the references to color in this figure legend, the reader is referred to the web version of this article.)

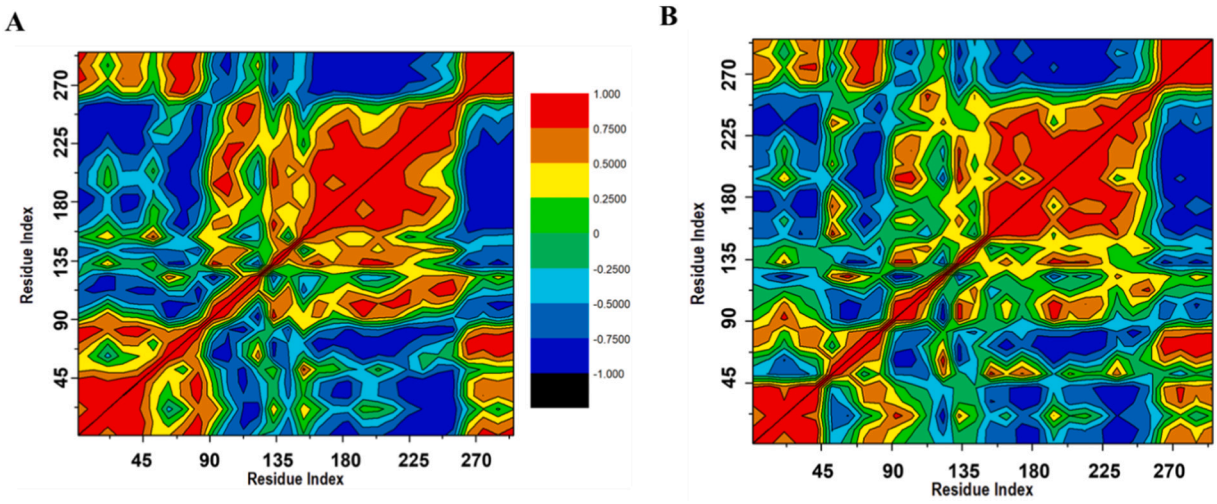

Fig. 5. Dynamics cross-correlation matrix analysis; (A) Apo CDK6 enzyme and (B) NAG-CDK6 complex calculated after 200 ns of MD trajectories.

superior inhibitory activity than apo CDK6.

3.3. Hydrogen bond analysis

Hydrogen bond analysis for intramolecular and intermolecular interactions is significant in the stable complexation. Overall numbers of intramolecular hydrogen bonds in the NAG-CDK6 complex were noted between 90 and 179, whereas 121–185 in CDK6, as displayed in Fig. 4A. The total number of intramolecular hydrogen bonds presented in apo CDK6 protein was lower than the NAG-CDK6 complex. We calculated the intermolecular hydrogen bonds for the NAG-CDK6 complex only, as shown in Fig. 4B. The numbers of hydrogen bonds in the NAG-CDK6 complex were 4 to 18, supported by the molecular docking analysis. This analysis accompanies all previous structural investigations [77].

3.4. Dynamic cross-correlation matrix

Dynamic cross-correlation matrix (DCCM) for the negative and positive correlation of all the amino acid residues for CDK6 and NAG-CDK6 complex were measured as shown in Fig. 5. The structure of CDK6 protein was distributed into numerous groups through positive and negative residual activities. Fig. 5A illustrates the residual activities that were highly negative and less positive in apo CDK6 protein in the resultant trajectories. The bound complex of NAG-CDK6 formed various correlated and less anti-correlated residual activities as distinguished from Fig. 5B. Noteworthy changes were observed in the NAG-CDK6 complex with highly correlated residual movements. In the structure of apo CDK6 protein, amino acid residues from 135 to 265 revealed the most anti-correlated residual movements, indicative of non-inhibitory activity of CDK6 protein without NAG. On the other side, exceptionally positive (red color) activities were observed from residues 1–45 and 266–290 in the NAG-CDK6 complex, indicating improved NAG inhibition to CDK6 protein.

3.5. MM/GBSA free binding energy analysis

Established from the trajectories, MM/GBSA energy calculations can provide detailed interpretations of the ligand binding to its target

Table 1
MM/GBSA-based binding energy profile of CDK6 in complex with NAG.

Complex	ΔE_{vdW}	ΔE_{ele}	ΔG_{gas}	ΔG_{polar}	$\Delta G_{nonpolar}$	ΔG_{sol}	ΔG_{bind}
CDK6-NAG	−41.24	−48.38	−72.68	68.59	−4.24	64.35	−45.36

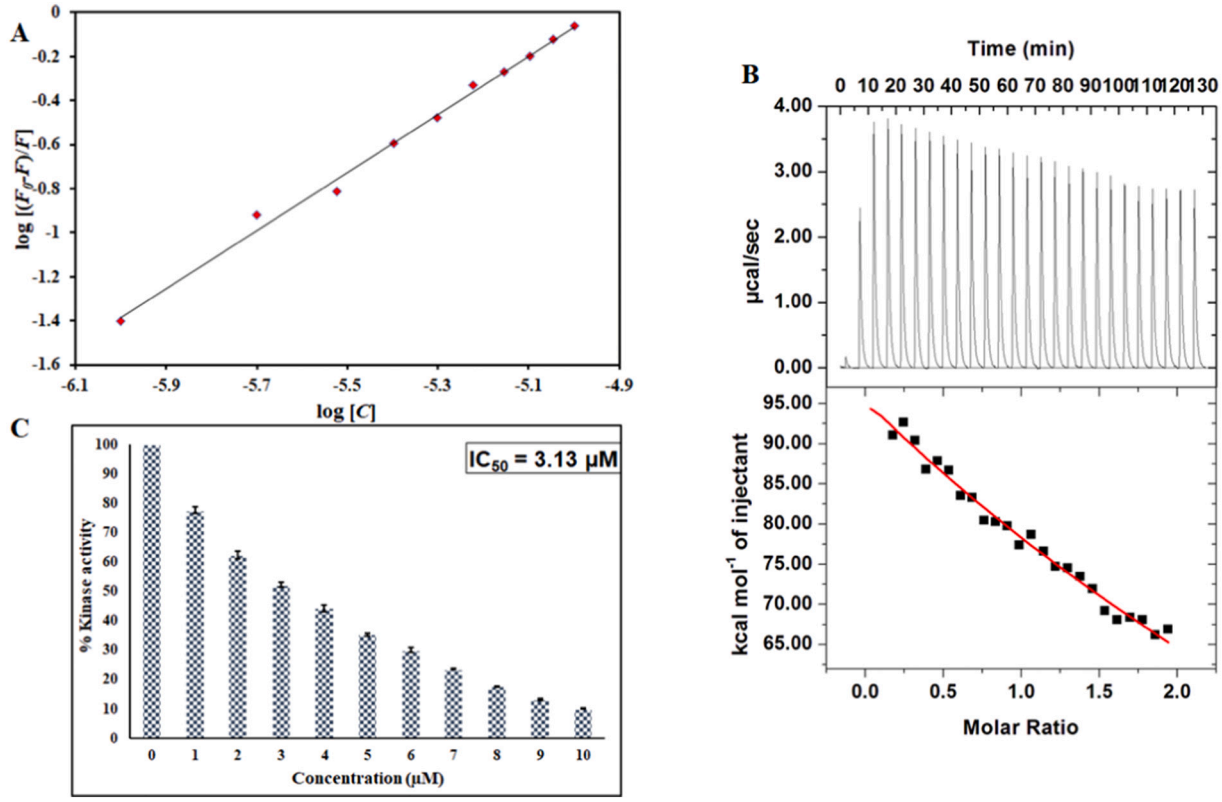

Fig. 6. (A) Modified Stern-Volmer plot of CDK6-NAG system. (B) ITC profile of CDK6-NAG system. (C) Kinase assay of CDK6 in the presence of varying NAG concentrations.

protein. This bound ligand can offer stable conformation to its corresponding protein. This analysis is critical to determine the binding affinity of NAG in complex with CDK6 protein to assess the function of NAG on CDK6 inhibition. The outcomes are presented in Table 1. Binding free energy (ΔG_{bind}) of NAG-CDK6 complex was noted with a −45.36 kcal/mol digital value and is the most negative energy. Other free energy components were assessed to illustrate the relationship between ligand-protein binding.

Significant contributions were achieved from the van der Waals and electrostatic energies in the NAG-CDK6 complex with binding scores of −41.24 and − 48.38 kcal/mol. The resulted electrostatic energy was more negative than the van der Waals energy. A considerable difference of −7.14 kcal/mol was calculated between this complex among these two energies. The ΔG_{gas} was the most negative energy in the NAG-CDK6 complex, with a −72.68 kcal/mol score. In the bound complex, ΔG_{sol} was the second most positive energy with a 64.35 kcal/mol score. The solvation energy was revealed as lower than the polar energy with 68.59 kcal/mol value. The least negative energy value of 4.24 kcal/mol was observed in the non-polar phase of the energy in the NAG bound complex. This discovery offers a valuable input in exploring the binding mechanism of NAG to CDK6 protein.

3.6. Fluorescence measurements

It was apparent from the above deployed computational approaches that NAG binds to CDK6, forming a stable complex. Thus, the next aim was to find if these observations are also validated by *in vitro* approaches. Fluorescence assay determine the actual binding affinity of NAG to CDK6. CDK6 was cloned, expressed, and purified (Fig. S1). CDK6 was titrated with increasing NAG concentrations. There was a decrease in the fluorescence of CDK6 with an increasing concentration of NAG, indicating that NAG binds to CDK6, forming a stable complex. This decrease is known as fluorescence quenching, and the obtained quenching data was put into the modified Stern-Volmer equations (Fig. 6A) to find the binding parameters of the CDK6-NAG complex. NAG binds to CDK6 with a binding constant (K) of 3.55×10^6 M^{-1}. This magnitude of the binding constant correlates with the binding constant reported earlier for other protein-ligand complexes, revealing the strong binding of NAG to CDK6.

3.7. Isothermal titration calorimetry

After we ascertained the actual binding affinity of NAG to CDK6 employing fluorescence assay, we next used ITC, one of the most sensitive techniques to study the interaction process. ITC provides valuable information regarding the mechanism of binding ligand to the protein finding the associated thermodynamic parameters of the system [78]. Fig. 6B depicts the ITC isotherm for the CDK6-NAG system obtained upon the titration of 200 µM NAG into 20 µM CDK6. The obtained isotherm advocates the spontaneous binding of NAG to CDK6. The positive heat deflection reveals the endothermic nature of the reaction. The upper panel shows the raw data obtained from the consecutive

Table 2
Binding and thermodynamic parameters of CDK6-NAG system obtained from ITC.

K_a (association constant) M^{-1}	ΔH (enthalpy change) cal/mol	ΔS (cal/mol/deg)
$K_a = 706 \pm 2.70 \times 10^4$	$\Delta H = 8.93 \times 10^5 \pm 3.01 \times 10^7$	$\Delta S = 3.01 \times 10^3$

injections of NAG into CDK6.

In contrast, the lower panel shows the binding curves attained after subtraction of heat of dilutions. K_a was found to be $706 \pm 2.70 \times 10^4$ M^{-1} indicating significant binding of NAG to CDK6. Many pieces of literature have reported that there might be variations in the obtained binding parameters from fluorescence spectroscopy and ITC. The apparent reason for these variations is that fluorescence spectroscopy measures local changes around fluorophores while ITC measures global changes in the protein [79].

Table 2 below shows the binding and thermodynamic parameters calculated by isothermal titration calorimetry.

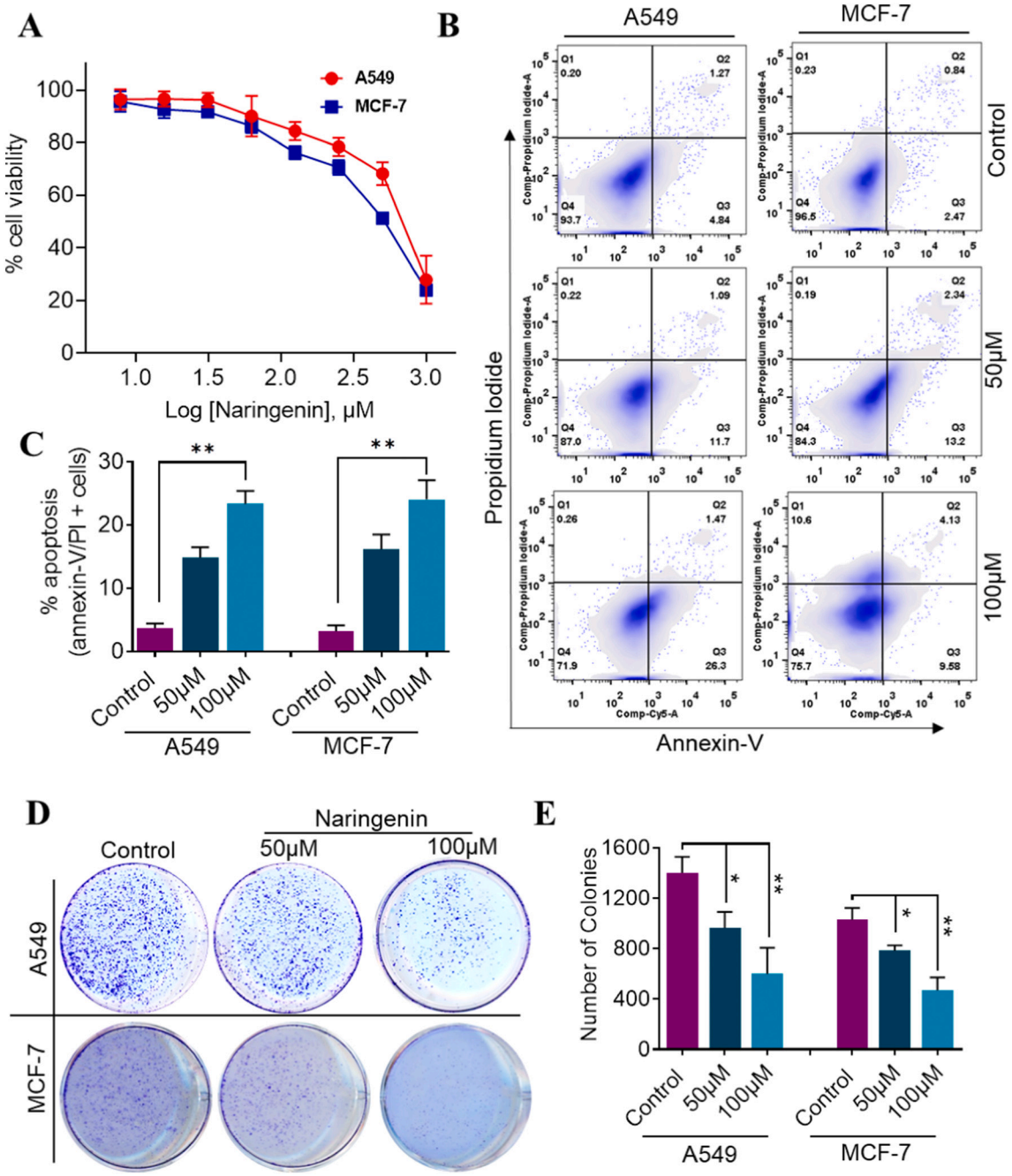

Fig. 7. NAG modulates the viability, apoptosis, and colonization of human cancer cells. (A) NAG decreased the viability of A549 and MCF-7 cells in a dose-dependent manner as assessed by MTT-assay following the 72 h treatment. (B) Flow cytometry analysis of the apoptotic potential of NAG in A549 and MCF-7 cells. The cells were incubated with NAG for 72 h, and following the treatment, the cells were stained with annexin-V/PI to see the apoptosis induction through flow cytometry. (C) Quantification of apoptosis in NAG treated A549 and MCF-7 cells (from n = 3 biological replicates). (D) Colony formation assay for A549 and MCF-7 cells under different concentrations of NAG. (E) The number of colonies as quantified in control and NAG treated A549 and MCF-7 cells. Significance of analysis was represented by *t*-test, *, $p < 0.05$; **, $p < 0.01$.

3.8. Enzyme inhibition assay

We confirmed the actual binding of NAG to CDK6 using fluorescence and ITC experiments. The next aim was to estimate the kinase activity of CDK6 in the presence of increasing NAG concentrations. The kinase activity of native CDK6 was taken as 100 % for reference purposes. Fig. 6C shows the kinase activity profile of CDK6 in the presence of varying NAG concentrations. A decrease in the kinase activity of CDK6 was observed with a corresponding increase in NAG concentrations. This decrease implies that NAG inhibits the kinase activity of CDK6. Hence, this inhibition effect can help to manage the disease driven by overexpression of CDK6. IC_{50} was 3.13 μM, suggesting NAG is a strong CDK6 inhibitor. Earlier studies have established other natural compounds as CDK6 inhibitors [57,60], and the IC_{50} obtained for NAG correlates to them. The value of this order has earlier been reported for other kinases, highlighting its importance. The importance of these inhibitors is attributable to the fact that kinases control various signaling pathways, and their altered expression is implicated in various pathological conditions. Thus, all the above experiments conclude that NAG is a potent inhibitor of CDK6 that can be used to manage CDK6-directed diseases.

3.9. Cell-based functional studies

NAG showed appreciable binding affinity and enzyme inhibition profile towards CDK6 (Figs. 1–6). Previous studies suggested that NAG acted as an anti-cancer molecule and showed promising outcomes in various cancers as a single molecule or in combinational approaches [80–82]. Interestingly, CDK6 was established as a potential anti-cancer drug target. Therefore, next, we have evaluated the anticancerous potential of NAG in human cancer cell lines that showed high CDK6 dependencies for their survival, such as A549 and MCF-7. First, we performed cell viability studies with NAG on selected cancer cell lines and observed that NAG treatment decreased the viability of A549 and MCF-7 cell lines in a dose-dependent manner (Fig. 7A).

Further, to evaluate the impact of NAG on the programmed cell death of cancer cells, we carried out annexin-V/PI staining. The results of annexin-V/PI staining suggested that NAG induces early to late apoptotic events in A549 and MCF-7 cells (Fig. 7B–C). To assess the impact of NAG on the colonization of cancer cells, we also performed a colony formation assay by incubating A549 and MCF-7 cells with NAG for 8–10 days and found that NAG decreases the colony formation ability of human cancer cells (Fig. 7D–E). The outcomes of cell-based studies are consistent with previous studies that showed that NAG showed promising anticancerous activities in multiple cancers [81,82]. In context to the impact of NAG on non-cancerous or normal human cells, it was established by various preclinical or clinical studies that NAG showed no adverse activities or side effects on normal human cells [81,83]. We observe that NAG showed desired activities at comparatively high doses (generally, >50 μM), which may limit the clinical implications of this molecule, however, the exciting feature of this molecule is that even at higher doses, it is safe for preclinical or clinical studies. To this end, various clinical trials are currently being under progress, and some were completed (ClinicalTrials.gov Identifier: NCT03582553) that showed that NAG had little or no toxicity towards normal cells [83]. Based on the observations of the present study, we demonstrated that NAG behaves as an effective inhibitor for CDK6, and owing to its CDK6 specific activities, it could be a promising molecule for combinational anti-cancer therapies in human malignancies that shows CDK6 specific vulnerabilities.

4. Conclusion

Cancer is among the leading death causes across the globe, having multiple manifestations. CDK6 overexpression is linked to various cancers, highlighting the crucial role of CDK6 inhibitors in anti-cancer therapeutics. Thus, we performed identification of potent CDK6 inhibitors among phytochemicals. The present study establishes NAG as a potential CDK6 inhibitor through an integrated *in-silico* and *in-vitro* experiments. The binding and conformational dynamics of CDK6-NAG were deciphered by MD simulation studies suggesting a stable CDK6-NAG complex. In addition, we observed that the binding of NAG doesn't cause any significant structural alterations in CDK6. The outcomes of fluorescence and ITC studies revealed an spontaneous binding of NAG to CDK6, leading to stable CDK6-NAG. Cell-based functional studies showed that NAG decreases the cell viability of human cancer cell lines, induces apoptosis, and reduces their colonization ability. The present study provides an additional axis towards utilizing NAG as a CDK6 inhibitor for the development of CDK6-targeted monotherapies or combinational therapeutic approaches.

Supplementary data to this article can be found online at https://doi.org/10.1016/j.ijbiomac.2022.06.013.

Funding

MIH acknowledges the Council of Scientific and Industrial Research for financial support [Project No. 27(0368)/20/EMR-II].

CRediT authorship contribution statement

MY: Conceptualization, writing-review and editing, Project Administration, Data Analysis, Investigation; **SK:** Data Curation, data validation, Resources, Visualization, software, Writing-review and editing; **AS:** Data validation, Data Analysis; Methodology, Investigation, Resources, writing-review and editing; **PK:** Methodology, Investigation, Writing-review and editing; **MS:** Data Curation, Writing-review and editing; **AME:** Investigation, Data Curation, Visualization, software, Writing-review and editing; **QMRH:** Visualization, software, Writing-review and editing; **MIH:** Data curation, Methodology, Visualization, Resources, formal analysis, Project Administration, writing-original draft.

Declaration of competing interest

The authors declare that they have no competing financial interests.

Acknowledgments

AME extends his appreciation to the Deanship of Scientific Research at Jouf University for funding his work through Research Grant Number (DSR-2021-01-0367). MIH thanks Department of Science and Technology, Government of India, for the FIST support (FIST program No. SR/FST/LSII/2020/782).

References

[1] L. Zhu, A.I. Skoultchi, Coordinating cell proliferation and differentiation, Curr. Opin. Genet. Dev. 11 (2001) 91–97.
[2] S. Ruijtenberg, S. van den Heuvel, Coordinating cell proliferation and differentiation: antagonism between cell cycle regulators and cell type-specific gene expression, Cell Cycle 15 (2016) 196–212.
[3] M. Malumbres, M. Barbacid, Cell cycle, CDKs and cancer: a changing paradigm, Nat. Rev. Cancer 9 (2009) 153–166.
[4] K.-C. Chou, Progresses in predicting post-translational modification, Int. J. Pept. Res. Ther. 26 (2020) 873–888.
[5] B. Lüscher, M. Bütepage, L. Eckei, S. Krieg, P. Verheugd, B.H. Shilton, ADP-ribosylation, a multifaceted post-translational modification involved in the control of cell physiology in health and disease, Chem. Rev. 118 (2018) 1092–1136.
[6] Z.-J. Han, Y.-H. Feng, B.-H. Gu, Y.-M. Li, H. Chen, The post-translational modification, SUMOylation, and cancer, Int. J. Oncol. 52 (2018) 1081–1094.
[7] M.A. Rahman, A.R. Krainer, O. Abdel-Wahab, SnapShot: splicing alterations in cancer, Cell 180 (2020), e201, 208–208.
[8] L. Chen, S. Liu, Y. Tao, Regulating tumor suppressor genes: post-translational modifications, Signal Transduct. Target. Ther. 5 (2020) 1–25.
[9] K. Alganem, A.-R. Hamoud, J.F. Creeden, N.D. Henkel, A.S. Imami, A.W. Joyce, J. B. Rethman, R. Shukla, S.M. O'Donovan, J. Meller, The active kinome: the modern view of how active protein kinase networks fit in biological research, Curr. Opin. Pharmacol. 62 (2022) 117–129.

[10] T.G. Cross, D. Scheel-Toellner, N.V. Henriquez, E. Deacon, M. Salmon, J.M. Lord, Serine/threonine protein kinases and apoptosis, Exp. Cell Res. 256 (2000) 34–41.
[11] S.J. Elledge, Cell cycle checkpoints: preventing an identity crisis, Science 274 (1996) 1664–1672.
[12] K.J. Barnum, M.J. O'Connell, Cell cycle regulation by checkpoints, in: Cell Cycle Control, Springer, 2014, pp. 29–40.
[13] X. Wu, X. Yang, Y. Xiong, R. Li, T. Ito, T.A. Ahmed, Z. Karoulia, C. Adamopoulos, H. Wang, L. Wang, Distinct CDK6 complexes determine tumor cell response to CDK4/6 inhibitors and degraders, Nat. Cancer 2 (2021) 429–443.
[14] F.A. Dick, S.M. Rubin, Molecular mechanisms underlying RB protein function, Nat. Rev. Mol. Cell Biol. 14 (2013) 297–306.
[15] C. Giacinti, A. Giordano, RB and cell cycle progression, Oncogene 25 (2006) 5220–5227.
[16] I. Foster, Cancer: a cell cycle defect, Radiography 14 (2008) 144–149.
[17] H. Wang, B.N. Nicolay, J.M. Chick, X. Gao, Y. Geng, H. Ren, H. Gao, G. Yang, J. A. Williams, J.M. Suski, The metabolic function of cyclin D3–CDK6 kinase in cancer cell survival, Nature 546 (2017) 426–430.
[18] A.S. Krall, H.R. Christofk, Division enzyme regulates metabolism, Nature 546 (2017) 357–358.
[19] D. Hanahan, R.A. Weinberg, Hallmarks of cancer: the next generation, Cell 144 (2011) 646–674.
[20] C.J. Sherr, D. Beach, G.I. Shapiro, Targeting CDK4 and CDK6: from discovery to therapy, Cancer Discov. 6 (2016) 353–367.
[21] S. Tadesse, M. Yu, M. Kumarasiri, B.T. Le, S. Wang, Targeting CDK6 in cancer: state of the art and new insights, Cell Cycle 14 (2015) 3220–3230.
[22] C. Guarducci, M. Bonechi, M. Benelli, C. Biagioni, G. Boccalini, D. Romagnoli, R. Verardo, R. Schiff, C.K. Osborne, C. De Angelis, Cyclin E1 and rb modulation as common events at time of resistance to palbociclib in hormone receptor-positive breast cancer, NPJ Breast Cancer 4 (2018) 1–10.
[23] K. Pandey, H.J. An, S.K. Kim, S.A. Lee, S. Kim, S.M. Lim, G.M. Kim, J. Sohn, Y. W. Moon, Molecular mechanisms of resistance to CDK4/6 inhibitors in breast cancer: a review, Int. J. Cancer 145 (2019) 1179–1188.
[24] D.S. Jairajpuri, T. Mohammad, K. Adhikari, P. Gupta, G.M. Hasan, M.F. Alajmi, M. T. Rehman, A. Hussain, M.I. Hassan, Identification of sphingosine Kinase-1 inhibitors from bioactive natural products targeting cancer therapy, ACS Omega 5 (2020) 14720–14729.
[25] P. Khan, A. Queen, T. Mohammad, N.S.Khan Smita, Z.B. Hafeez, M.I. Hassan, S. Ali, Identification of α-mangostin as a potential inhibitor of microtubule affinity regulating kinase 4, J. Nat. Prod. 82 (2019) 2252–2261.
[26] S. Khan, F.A. Alhumaydhi, M.S. Khan, S.E. Sharaf, W. Al Abdulmonem, M. I. Hassan, A. Shamsi, D. Kumar Yadav, Exploring binding mechanism of naringenin to human transferrin using combined spectroscopic and computational methods: towards therapeutic targeting of neurodegenerative diseases, J. Mol. Liq. 356 (2022), 119001.
[27] T. Mohammad, F.I. Khan, K.A. Lobb, A. Islam, F. Ahmad, M.I. Hassan, Identification and evaluation of bioactive natural products as potential inhibitors of human microtubule affinity-regulating kinase 4 (MARK4), J. Biomol. Struct. Dyn. 37 (2019) 1813–1829.
[28] T. Mohammad, S. Siddiqui, A. Shamsi, M.F. Alajmi, A. Hussain, A. Islam, F. Ahmad, M.I. Hassan, Virtual screening approach to identify high-affinity inhibitors of serum and glucocorticoid-regulated kinase 1 among bioactive natural products: combined molecular docking and simulation studies, Molecules 25 (2020).
[29] A. Beg, F.I. Khan, K.A. Lobb, A. Islam, F. Ahmad, M.I. Hassan, High throughput screening, docking, and molecular dynamics studies to identify potential inhibitors of human calcium/calmodulin-dependent protein kinase IV, J. Biomol. Struct. Dyn. 37 (2019) 2179–2192.
[30] P. Gupta, S. Khan, Z. Fakhar, A. Hussain, M.T. Rehman, M.F. AlAjmi, A. Islam, F. Ahmad, M.I. Hassan, Identification of potential inhibitors of Calcium/ Calmodulin-dependent protein kinase IV from bioactive phytoconstituents, Oxidative Med. Cell. Longev. 16 (2020).
[31] H. Naz, M. Tarique, S. Ahamad, M.F. Alajmi, A. Hussain, M.T. Rehman, S. Luqman, M.I. Hassan, Hesperidin-CAMKIV interaction and its impact on cell proliferation and apoptosis in the human hepatic carcinoma and neuroblastoma cells, J. Cell. Biochem. 120 (2019) 15119–15130.
[32] H. Naz, M. Tarique, P. Khan, S. Luqman, S. Ahamad, A. Islam, F. Ahmad, M. I. Hassan, Evidence of vanillin binding to CAMKIV explains the anti-cancer mechanism in human hepatic carcinoma and neuroblastoma cells, Mol. Cell. Biochem. 438 (2018) 35–45.
[33] D.M. Kopustinskiene, V. Jakstas, A. Savickas, J. Bernatoniene, Flavonoids as anti-cancer agents, Nutrients 12 (2020) 457.
[34] Z. Ping, Y. Peng, H. Lang, C. Xinyong, Z. Zhiyi, W. Xiaocheng, Z. Hong, S. Liang, Oxidative stress in radiation-induced cardiotoxicity, Oxidative Med. Cell. Longev. 2020 (2020).
[35] I. Koçak, S. Sarac, E. Aydogan, E. Şentürk, D. Akakın, K. Koroglu, Ö. Özer, Evaluation of the possible protective role of naringenin on gentamicin-induced ototoxicity: a preliminary study, Int. J. Pediatr. Otorhinolaryngol. 100 (2017) 247–253.
[36] R.J. Nijveldt, E. Van Nood, D.E. Van Hoorn, P.G. Boelens, K. Van Norren, P.A. Van Leeuwen, Flavonoids: a review of probable mechanisms of action and potential applications, Am. J. Clin. Nutr. 74 (2001) 418–425.
[37] L.J. Wilcox, N.M. Borradaile, M.W. Huff, Antiatherogenic properties of naringenin, a citrus flavonoid, Cardiovasc. Drug Rev. 17 (1999) 160–178.
[38] P.Venkateswara Rao, S. Kiran, P. Rohini, P. Bhagyasree, Flavonoid: a review on Naringenin, J. Pharmacogn. Phytochem. 6 (2017) 2778–2783.
[39] K. Patel, G.K. Singh, D.K. Patel, A review on pharmacological and analytical aspects of naringenin, Chin. J. Integr. Med. 24 (2018) 551–560.
[40] R.H. Moghaddam, Z. Samimi, S.Z. Moradi, P.J. Little, S. Xu, M.H. Farzaei, Naringenin and naringin in cardiovascular disease prevention: a preclinical review, Eur. J. Pharmacol. 173535 (2020).
[41] E. Hernández-Aquino, P. Muriel, Beneficial effects of naringenin in liver diseases: molecular mechanisms, World J. Gastroenterol. 24 (2018) 1679.
[42] M. Zhao, C. Li, F. Shen, M. Wang, N. Jia, C. Wang, Naringenin ameliorates LPS-induced acute lung injury through its anti-oxidative and anti-inflammatory activity and by inhibition of the PI3K/AKT pathway, Exp. Ther. Med. 14 (2017) 2228–2234.
[43] S. Li, Y. Zhang, Y. Sun, G. Zhang, J. Bai, J. Guo, X. Su, H. Du, X. Cao, J. Yang, Naringenin improves insulin sensitivity in gestational diabetes mellitus mice through AMPK, Nutr. Diabetes 9 (2019) 1–10.
[44] R. Zhao, H. Xiao, T. Jin, F. Xu, Y. Li, H. Li, Z. Zhang, Y. Zhang, Naringenin promotes cell autophagy to improve high-fat-diet-induced atherosclerosis in ApoE-/-mice, Braz. J. Med. Biol. Res. 54 (2021).
[45] Z. Namkhah, F. Naeini, S. Mahdi Rezayat, M. Yaseri, S. Mansouri, M. Javad Hosseinzadeh-Attar, Does naringenin supplementation improve lipid profile, severity of hepatic steatosis and probability of liver fibrosis in overweight/obese patients with NAFLD? A randomised, double-blind, placebo-controlled, clinical trial, Int. J. Clin. Pract. 75 (2021), e14852.
[46] Z. Zhao, G. Jin, Y. Ge, Z. Guo, Naringenin inhibits migration of breast cancer cells via inflammatory and apoptosis cell signaling pathways, Inflammopharmacology 27 (2019) 1021–1036.
[47] Z. Memariani, S.Q. Abbas, S.S. Ul Hassan, A. Ahmadi, A. Chabra, Naringin and naringenin as anti-cancer agents and adjuvants in cancer combination therapy: efficacy and molecular mechanisms of action, a comprehensive narrative review, Pharmacol. Res. 171 (2021), 105264.
[48] V. Nachammai, S. Jeyabalan, S. Muthusamy, Anxiolytic effects of silibinin and Naringenin on zebrafish model: a preclinical study, Indian J. Pharmacol. 53 (2021).
[49] M. Ghanbari-Movahed, G. Jackson, M.H. Farzaei, A. Bishayee, A systematic review of the preventive and therapeutic effects of naringin against human malignancies, Front. Pharmacol. 12 (2021) 250.
[50] O.-G. Issinger, B. Guerra, Phytochemicals in cancer and their effect on the PI3K/ AKT-mediated cellular signalling, Biomed. Pharmacother. 139 (2021), 111650.
[51] S. Rajabi, S. Noori, M.R. Ashrafi, M.A. Movahed, S. Farzaneh, A. Zarghi, Naringenin Enhances Anti-Proliferation Effect of FMSP On K562 Human Chronic Myelogenous Leukemia Cells Via Targeting Calmodulin Signaling Pathway, 2021.
[52] J. Li, J. Zhao, H. Zhang, M. Liu, X. Li, Naringin Suppressing the PI3K/Akt Signaling Pathway as a Drug Target in BIU87 Cells, 2020.
[53] W. Zeng, L. Jin, F. Zhang, C. Zhang, W. Liang, Naringenin as a potential immunomodulator in therapeutics, Pharmacol. Res. 135 (2018) 122–126.
[54] B. Pateliya, V. Burade, S. Goswami, Combining naringenin and metformin with doxorubicin enhances anti-cancer activity against triple-negative breast cancer in vitro and in vivo, Eur. J. Pharmacol. 891 (2021), 173725.
[55] Z. Zhu, L. Cui, J. Yang, C.T. Vong, Y. Hu, J. Xiao, G. Chan, Z. He, Z. Zhong, Anticancer effects of asiatic acid against doxorubicin-resistant breast cancer cells via an AMPK-dependent pathway in vitro, Phytomedicine 92 (2021), 153737.
[56] S. Anwar, S. Khan, A. Shamsi, F. Anjum, A. Shafie, A. Islam, F. Ahmad, M.I. Hassan, Structure-based investigation of MARK4 inhibitory potential of naringenin for therapeutic management of cancer and neurodegenerative diseases, J. Cell. Biochem. 122 (10) (2021) 1445–1459..
[57] M. Yousuf, A. Shamsi, P. Khan, M. Shahbaaz, M.F. AlAjmi, A. Hussain, G. M. Hassan, A. Islam, Q.M.Rizwanul Haque, M. Hassan, Ellagic acid controls cell proliferation and induces apoptosis in breast cancer cells via inhibition of cyclin-dependent kinase 6, Int. J. Mol. Sci. 21 (2020) 3526.
[58] M. Karmakar, C.H. Rodrigues, K.E. Holt, S.J. Dunstan, J. Denholm, D.B. Ascher, Empirical ways to identify novel bedaquiline resistance mutations in AtpE, PloS one 14 (2019), e0217169.
[59] J. Feng, Y. Chen, J. Pu, X. Yang, C. Zhang, S. Zhu, Y. Zhao, Y. Yuan, H. Yuan, F. Liao, An improved malachite green assay of phosphate: mechanism and application, Anal. Biochem. 409 (2011) 144–149.
[60] M. Yousuf, A. Shamsi, A. Queen, M. Shahbaaz, P. Khan, A. Hussain, M.F. Alajmi, Q. M. Rizwanul Haque, M. Imtaiyaz Hassan, Targeting cyclin-dependent kinase 6 by vanillin inhibits proliferation of breast and lung cancer cells: combined computational and biochemical studies, J. Cell. Biochem. 122 (8) (2021) 897–910.
[61] M. Yousuf, P. Khan, A. Shamsi, M. Shahbaaz, G.M. Hasan, Q.M.R. Haque, A. Christoffels, A. Islam, M.I. Hassan, Inhibiting CDK6 activity by quercetin is an attractive strategy for cancer therapy, ACS Omega 5 (2020) 27480–27491.
[62] N.S. Khan, P. Khan, A. Inam, K. Ahmad, M. Yousuf, A. Islam, S. Ali, A. Azam, M. Husain, M.I. Hassan, Discovery of 4-(2-(dimethylamino) ethoxy) benzohydrazide derivatives as prospective microtubule affinity regulating kinase 4 inhibitors, RSC Adv. 10 (2020) 20129–20137.
[63] A. Das Mahapatra, A. Queen, M. Yousuf, P. Khan, A. Hussain, M.T. Rehman, M. F. Alajmi, B. Datta, M.I. Hassan, Design and development of 5-(4H)-oxazolones as potential inhibitors of human carbonic anhydrase VA: towards therapeutic management of diabetes and obesity, J. Biomol. Struct. Dyn. (2020) 1–11.
[64] G. Madhavi Sastry, M. Adzhigirey, T. Day, R. Annabhimoju, W. Sherman, Protein and ligand preparation: parameters, protocols, and influence on virtual screening enrichments, J. Comput. Aided Mol. Des. 27 (2013) 221–234.
[65] T.-S. Lee, D.S. Cerutti, D. Mermelstein, C. Lin, S. LeGrand, T.J. Giese, A. Roitberg, D.A. Case, R.C. Walker, D.M. York, GPU-accelerated molecular dynamics and free energy methods in Amber18: performance enhancements and new features, J. Chem. Inf. Model. 58 (2018) 2043–2050.

[66] A. Perez, J.L. MacCallum, E. Brini, C. Simmerling, K.A. Dill, Grid-based backbone correction to the ff12SB protein force field for implicit-solvent simulations, J. Chem. Theory Comput. 11 (2015) 4770–4779.
[67] J. Wang, W. Wang, P.A. Kollman, D.A. Case, Automatic atom type and bond type perception in molecular mechanical calculations, J. Mol. Graph. Model. 25 (2006) 247–260.
[68] D.R. Roe, T.E. Cheatham III, PTRAJ and CPPTRAJ: software for processing and analysis of molecular dynamics trajectory data, J. Chem. Theory Comput. 9 (2013) 3084–3095.
[69] E. Seifert, OriginPro 9.1: scientific data analysis and graphing software-software review, J. Chem. Inf. Model. 54 (2014) 1552.
[70] E. Wang, H. Sun, J. Wang, Z. Wang, H. Liu, J.Z. Zhang, T. Hou, End-point binding free energy calculation with MM/PBSA and MM/GBSA: strategies and applications in drug design, Chem. Rev. 119 (2019) 9478–9508.
[71] M. Yousuf, A. Shamsi, P. Khan, M. Shahbaaz, M.F. AlAjmi, A. Hussain, G. M. Hassan, A. Islam, Q.M. Rizwanul Haque, M.I. Hassan, Ellagic acid controls cell proliferation and induces apoptosis in breast cancer cells via inhibition of cyclin-dependent kinase 6, Int. J. Mol. Sci. 21 (2020).
[72] P. Gupta, T. Mohammad, R. Dahiya, S. Roy, O.M.A. Noman, M.F. Alajmi, A. Hussain, M.I. Hassan, Evaluation of binding and inhibition mechanism of dietary phytochemicals with sphingosine kinase 1: towards targeted anti-cancer therapy, Sci. Rep. 9 (2019) 019–55199.
[73] P. Gupta, T. Mohammad, P. Khan, M.F. Alajmi, A. Hussain, M.T. Rehman, M. I. Hassan, Evaluation of ellagic acid as an inhibitor of sphingosine kinase 1: a targeted approach towards anti-cancer therapy, Biomed. Pharmacother. 118 (2019) 25.
[74] F.I. Khan, K. Bisetty, K.R. Gu, S. Singh, K. Permaul, M.I. Hassan, D.Q. Wei, Molecular dynamics simulation of chitinase I from thermomyces lanuginosus SSBP to ensure optimal activity, Mol. Simul. 43 (2017) 480–490.
[75] S. Khan, Z. Fakhar, A. Hussain, A. Ahmad, D.S. Jairajpuri, M.F. Alajmi, M.I. Hassan, Structure-based identification of potential SARS-CoV-2 main protease inhibitors, J. Biomol. Struct. Dyn. 19 (2020) 1–14.
[76] S.A. Khan, K. Zia, S. Ashraf, R. Uddin, Z. Ul-Haq, Identification of chymotrypsin-like protease inhibitors of SARS-CoV-2 via integrated computational approach, J. Biomol. Struct. Dyn. 39 (2021) 2607–2616.
[77] H. Chen, A.Z. Panagiotopoulos, Molecular modeling of surfactant micellization using solvent-accessible surface area, Langmuir 35 (2019) 2443–2450.
[78] A. Shamsi, A. Ahmed, M.S. Khan, M. Al Shahwan, F.M. Husain, B. Bano, Understanding the binding between rosmarinic acid and serum albumin: in vitro and in silico insight, J. Mol. Liq. 311 (2020), 113348.
[79] A. Shamsi, S. Anwar, T. Mohammad, M.F. Alajmi, A. Hussain, M. Rehman, G. M. Hasan, A. Islam, M. Hassan, MARK4 inhibited by AChE inhibitors, donepezil and rivastigmine tartrate: insights into Alzheimer's disease therapy, Biomolecules 10 (2020) 789.
[80] H. Xiong, Z. Chen, B. Lin, B. Xie, X. Liu, C. Chen, Z. Li, Y. Jia, Z. Wu, M. Yang, Naringenin regulates FKBP4/NR3C1/NRF2 Axis in autophagy and proliferation of breast cancer and differentiation and maturation of dendritic cell, Front. Immunol. 12 (2021).
[81] J. Fernandez, B. Silvan, R. Entrialgo-Cadierno, C.J. Villar, R. Capasso, J.A. Uranga, F. Lombo, R. Abalo, Antiproliferative and palliative activity of flavonoids in colorectal cancer, Biomed. Pharmacother. 143 (2021), 112241.
[82] G.-Y. Lian, Q.-M. Wang, T.S.-K. Mak, X.-R. Huang, X.-Q. Yu, H.-Y. Lan, Inhibition of tumor invasion and metastasis by targeting TGF-β-smad-MMP2 pathway with asiatic acid and naringenin, Mol. Ther. Oncolytics 20 (2021) 277–289.
[83] B. Salehi, P.V.T. Fokou, M. Sharifi-Rad, P. Zucca, R. Pezzani, N. Martins, J. Sharifi-Rad, The therapeutic potential of naringenin: a review of clinical trials, Pharmaceuticals 12 (2019) 11.